Sc_9Te_2: A Two-Dimensional Distortion Wave in the Scandium-Richest Telluride

Paul A. Maggard and John D. Corbett*

Contribution from the Department of Chemistry, Iowa State University, Ames, Iowa 50011

Received September 13, 1999

Abstract: Sc_9Te_2 was prepared by high-temperature solid-state techniques, and the structure was determined by single-crystal X-ray diffraction to be monoclinic, *Cc* (No. 9, $Z = 8$) with $a = 7.7576(1)$ Å, $b = 15.654(3)$ Å, $c = 17.283(3)$ Å, and $\beta = 90.01(3)°$ at 23 °C. The structure of metallic Sc_9Te_2 can be viewed as columns built either from distorted 3×3 bcc metal atoms or from distorted edge-sharing octahedra along $\vec{a}$ that are joined via intercolumn bonds on opposite sides into two-dimensional layers along $\vec{b}$. A corrugated layer of Te atoms separates the metal layers in the *c* direction. This structure derives from the Ti_9Se_2 structure, with doubled *a* and *b* dimensions and a lower symmetry. Magnetic susceptibility measurements on Sc_9Te_2 show a substantially temperature-independent paramagnetism that is much smaller per metal atom than those for other scandium-rich tellurides or scandium metal. Extended Hückel band calculations reveal a clear distinction between high overlap populations for Sc−Sc interactions in the interior of the condensed metal structure and lower values for those on the exterior that have Te neighbors. The distortion generally enhances the overlap populations of occupied states.

Introduction

The nature of metal−metal bonding has been an important aspect of inorganic chemistry since the days of Pauling.[1] Metal−metal bonding in low-dimensional structures has been cited as a key component in synthesizing materials that contain metal-lattice modulations or charge density waves.[2,3] The study of metal−metal bonding in early transition-metal compounds, chalcogenides especially, has received increased attention over the past 30 years. Voluminous expressions of lower-dimensional metal−metal bonding have been uncovered in such examples as Ti_8Ch_3[4,5] and Ti_2Ch[6,7] (Ch = S, Se), $Ti_{11}Se_4$,[8] Ti_9Se_2,[9] Ti_5Te_4,[10] Hf_2Te,[11] Hf_3Te_2,[12] Hf_2Se_3,[13] Zr_3Te,[14] Zr_5Te_4,[15] and Zr_2Te.[16] This chemistry has only recently been extended to the earliest and electron-poorest transition metals, namely, Sc_2Te[17] and R_8Te_3 (R = Sc, Y).[18] Structural and bonding relationships among these electron-impoverished tellurides and the electron-richer Ti, Zr, and Hf chalcogenides have given good insights regarding the importance of atom sizes, valence electron concentrations, and metal to nonmetal proportions in the determination of stability and structural features.

Often little insight can be offered about the bonding or other features that drive the structural outcomes. One might think that well-established interrelationships between electron counts, steric/matrix effects, and bond distances upon which the foundation of rational chemistry is based are too complex to be understood. However, the interrelationships previously outlined[18] for one case, M_8Ch_3, have proven valuable in understanding the chemistry. A great many of the metal-rich phases can be described as chains of octahedra sharing vertexes or edges that may be further condensed in diverse ways into infinite single, double, or quadruple chains. The majority (>95%) of these metal-rich phases share one common feature, a short repeat axis that appears to be determined primarily by the van der Waals radii of the anions. The metal−metal bonds repeat along this short axis as well, but these distances are usually determined by anion−anion contacts. Additionally, neighboring metal atoms often occupy alternating positions along the short axis, for example, at $^1/_4$ and $^3/_4$, and this arrangement may have a distinct impact on all metal−metal distances. As for Sc_8Te_3 versus $Ti_8(S,Se)_3$, a cooperative result of the effects of metal-based electron counts (valence electron concentration per atom, VEC), anion sizes, and the degree of M−M bonding appear to be involved. An increase in VEC plus a decrease in anion size together afford more short metal−metal contacts and bonding. This effect seems to be at work in the present Sc_9Te_2, which is related to Ti_9Se_2[9] via a predicted discontinuous symmetry-lowering metal lattice distortion. This article also presents an analysis of the electronic structures and

(1) Pauling, L. *Phys. Rev*. **1938**, *54*, 899. Pauling, L. *The Nature of the Chemical Bond;* Cornell University Press: Ithaca, NY, 1960; p 400.
(2) Whangbo, M. H.; Canadell, E.; Foury, P. *Science* **1991**, *252*, 96.
(3) Thorne, R. E. *Phys. Today* **1996**, *49*, 42.
(4) Owens, J. P.; Franzen, H. F. *Acta Crystallogr*. **1974**, *B30*, 427.
(5) Weirich, T. E.; Pöttgen, R.; Simon, A. *Z. Kristallogr*. **1996**, *211*, 929.
(6) Owens, J. P.; Conard, B. R.; Franzen, H. F. *Acta Crystallogr*. **1967**, *23*, 77.
(7) Weirich, T. E.; Pöttgen, R.; Simon, A. *Z. Kristallogr*. **1996**, *211*, 928.
(8) Weirich, T. E.; Ramlau, R.; Simon, A.; Hovmöller, S.; Zou, X. *Nature* **1996**, *382*, 144.
(9) Weirich, T. E.; Simon, A.; Pöttgen, R. *Z. Anorg. Allg. Chem.* **1996**, *622*, 630.
(10) Gronvold, F.; Kjekshus, A.; Raaum, F. *Acta Crystallogr*. **1961**, *14*, 930.
(11) Harbrecht, B.; Conrad, M.; Degen, T.; Herbertz, R. *J. Alloys Compd*. **1997**, *255*, 178.
(12) Abdon, R. L.; Hughbanks, T. *Angew. Chem., Int. Ed. Engl*. **1994**, *33*, 2414.
(13) Schewe-Miller, I. M.; Young, Y. G. *J. Alloys Compd*. **1994**, *216*, 113.
(14) Harbrecht, B.; Leersch, R. *J. Alloys Compd*. **1996**, *238*, 13.
(15) Brattas, L.; Kjekshus, A. *Acta Chem. Scand*. **1971**, *25*, 2350.
(16) Orlygsson, G.; Harbrecht, B. *Inorg. Chem.* **1999**, *38*, 3377.
(17) Maggard, P. A.; Corbett, J. D. *Angew. Chem., Int. Ed. Engl*. **1997**, *36*, 1974.
(18) Maggard, P. A.; Corbett, J. D. *Inorg. Chem.* **1998**, *37*, 814.

10.1021/ja993316j CCC: $19.00
Published on Web 01/21/2000

Table 1. Single-Crystal X-ray Data Collection and Refinement Parameters for Sc_9Te_2

formula weight	659.84
space group, Z	Cc (No. 9), 8
lattice parameters and cell volume	
a (Å)	7.7576(1)
b (Å)	15.654(3)
c (Å)	17.283(3)
β (deg)	90.01(3)
V (Å^3)	2098.8(6)
d_{calc} (g/cm^3)	4.176
μ (Mo Kα) (cm^{-1})	108.10
residuals $R1$, w$R2$ ($\times 100$)[a]	3.1; 9.8

[a] $R1 = \sum||F_o| - |F_c||/\sum|F_o|$; w$R2 = [\sum w(|F_o|^2 - |F_c|^2)^2/\sum w(|F_o|^2)^2]^{1/2}$, $w = 1/(\sigma_F^2)^2$.

distortion wave that relates Ti_9Se_2 to Sc_9Te_2, the metal-richest binary telluride known among the electron-poorest transition metals.

Experimental Section

Syntheses. All materials were handled in a He-filled glovebox. The synthesis of Sc_9Te_2 began with the preparation of Sc_2Te_3 (NaCl type with disordered cation vacancies). The elements as received (Sc turnings 99.7%, Aldrich-APL; Te powder, 99.99%, Alfa-AESAR) were loaded in a 2:3 stoichiometry into a fused silica container. This was evacuated, sealed, and heated to 450 °C for 12 h, and then to 900 °C for 72 h. Guinier film data confirmed the production of only the target product. This and the appropriate amount of scandium turnings to give a 9:2 stoichiometry were then pelletized with a hydraulic press within a glovebox. The pellet was arc-melted in the glovebox for 20 s/side with a current of 70 A. A Guinier pattern of the product at this point revealed single-phase (>95%) monoclinic Sc_9Te_2. This was annealed at 1135 °C for 72 h inside a welded tantalum container and then allowed to cool radiatively. It should be noted that still higher annealing temperatures resulted in reaction of the sample with and subsequent failure of the tantalum tubing. After annealing, powder diffraction data revealed that Sc_9Te_2 had been obtained in evidently quantitative yield, and single crystals therein were selected for structural analysis. We have not been able to prepare a Y_9Te_2 analogue.

Single-Crystal Diffraction. Several black, irregularly shaped crystals were mounted inside 0.3-mm i.d. glass capillaries. Crystal qualities were checked with Laue photographs, and the best crystal was taken for a data set collection on a Bruker CCD diffractometer operating at room temperature with Mo Kα_1 radiation. Ninety reflection frames collected with 15-s exposures were analyzed and yielded an orthorhombic unit cell with $a = 7.821$ Å, $b = 17.285$ Å, and $c = 3.879$ Å, with a few weak reflections not included. This cell was the same as that obtained earlier from diffractometers equipped with point detectors, from which a Ti_9Se_2-type structure (*Pnma*) had been solved, but with much apparent disorder (some extreme ellipsoids). A set of 90 reflection frames recollected with 45-s exposures revealed additional reflections that doubled both the a and c axes and gave $a = 7.7576$ (3) Å, $b = 15.654$ (3) Å, and $c = 17.283$ (3) Å in the standard setting. One sphere of reflections ($\pm h$, $\pm k$, $\pm l$) was collected to $2\theta \sim 56°$. The reflection frames when integrated and filtered with SAINTPLUS[19] gave 7239 reflections, of which 2141 were unique and observed ($I > 3\sigma_I$). A comparison of reflection intensities clearly demonstrated that there was no mirror plane normal to a (or c), which with the distorted supercell reduces the original *Pnma* to monoclinic *Cc*. An absorption correction was applied with the package program SADABS.[20] Additional observational conditions suggested the possible space group *Cc*. Structural models were obtained and successfully refined with the SHELXTL[21] program. Some data collection and refinement parameters are given in Table 1. The refinement converged at $R1$/w$R2 = 0.031/0.098$. For the subcell, 1069 observed unique reflections yielded $R1$/w$R2 = 0.030/0.088$, while 1072 observed reflections unique to the supercell gave $R1$/w$R2 = 0.040/0.110$. On average, the subcell reflections were about 3 times the intensity of the unique supercell data. The complete positional and isotropic-equivalent thermal parameters for Sc_9Te_2 are given in Table 2. Additional data collection, refinement and anisotropic displacement parameters, and all interatomic distances are given in the Supporting Information. These as well as the F_o/F_c listing are available from J.D.C.

Table 2. Positional and Isotropic-Equivalent Thermal Parameters for Sc_9Te_2

atom[a]	x	y	z	U_{eq}(Å^2)[b]
Te1	0.96968(8)	0.38090(4)	0.98396(4)	0.0080(2)
Te2	0.96841(9)	0.62951(3)	0.88165(4)	0.0061(2)
Te3	0.46538(9)	0.62949(3)	0.88165(4)	0.0062(2)
Te4	0.46386(8)	0.38088(4)	0.98397(4)	0.0082(2)
Sc1[1]	0.7179(3)	0.4849(1)	0.8945(1)	0.0074(5)
Sc2[1]	0.2174(3)	0.4759(1)	0.8819(2)	0.0073(5)
Sc3[1]	0.2178(4)	0.2260(1)	0.9855(2)	0.0076(5)
Sc4[1]	0.2178(4)	0.7350(1)	0.9743(2)	0.0080(5)
Sc5[2]	0.7156(3)	0.6808(1)	0.7633(2)	0.0083(5)
Sc6[2]	0.7152(3)	0.4316(2)	0.1025(2)	0.0076(5)
Sc7[2]	0.2155(3)	0.4245(1)	0.1089(1)	0.0090(5)
Sc8[2]	0.2157(3)	0.6741(1)	0.7576(1)	0.0071(5)
Sc9[3]	0.9908(3)	0.5740(1)	0.0469(1)	0.0102(5)
Sc10[3]	0.9905(3)	0.8247(1)	0.8200(1)	0.0093(5)
Sc11[3]	0.9409(3)	0.3247(1)	0.8198(1)	0.0085(5)
Sc12[3]	0.4406(3)	0.5740(1)	0.0470(1)	0.0098(5)
Sc13[4]	0.4918(3)	0.2624(1)	0.1272(1)	0.0101(5)
Sc14[4]	0.4927(3)	0.5120(1)	0.7389(1)	0.0109(5)
Sc15[4]	0.9389(3)	0.2623(1)	0.1272(1)	0.0080(5)
Sc16[4]	0.9375(3)	0.4881(1)	0.2388(1)	0.0081(5)
Sc17[5]	0.2166(4)	0.6147(1)	0.1994(2)	0.0078(4)
Sc18[5]	0.7166(4)	0.3651(1)	0.6660(2)	0.0089(4)

[a] Superscripts 1−5 denote corresponding metal positions within the Ti_9Se_2 structure. [b] $U_{eq} = (1/3)\sum_i\sum_j U_{ij}a_i^*a_j^*\vec{a}_i\vec{a}_j$.

Properties. A weighed, powdered sample of ~50 mg of Sc_9Te_2 was loaded inside the glovebox so that it was sandwiched between two close-fitting rods inside a 5-mm o.d. fused silica tube. Magnetizations of the samples were measured from 6 to 300 K at a field of 3 T with a Quantum Design MPMS SQUID magnetometer. Also, the magnetization versus field properties were checked at 80 and 160 K, and the M values were found to intercept $M = 0$ at $H = 0$, suggesting that the temperature dependences are intrinsic, the same as those determined earlier for the other scandium-rich phases. The data were corrected for the diamagnetism of both the sample holder and the atom cores.

Resistivities of powdered ~50-mg samples of Sc_9Te_2 diluted with Al_2O_3 powder were measured with a "Q" apparatus at ~35 MHz between 100 and 300 K.

Band Calculations. Extended Hückel band calculations were carried out within the tight-binding approximation[22] for the full structure of Sc_9Te_2 at 75 k points spread out over the irreducible wedge. H_{ii} parameters employed were those values iterated to charge consistency for Sc_2Te (eV):[17] Sc 4s, −6.75; 4p, −3.38; 3d, −6.12. Te 6s, −21.20; 6p, −12.00.

Results and Discussion

Structural Description. A near-[100] section of the Sc_9Te_2 structure is shown in Figure 1, and the more significant (nearest neighbor) scandium−scandium distances are given in Table 3. The atom distribution can be viewed as corrugated multilayers of scandium atoms (white) that stack normal to $\vec{c}$ and are separated into two-dimensional (2D) sheets by isolated tellurium atoms (gray). The most conspicuous building block of the metal substructure is approximately a one-dimensional (1D) square column of scandium, three atoms in width and height, that extends infinitely along $\vec{a}$. Adjoining columns are identical but displaced by $a/2$, which allows the display of all independent atom numbers as these alternate along the columns. This 3 × 3

(19) *SAINTPLUS*; Bruker AXS, Inc.: Madison, WI, 1996.
(20) Blessing, R. H. *Acta Crystallogr.* **1995**, *A51*, 33.
(21) Sheldrick, G. M. *SHELXS-86*; Universität Göttingen: Germany, 1986.
(22) Hoffman, R. *J. Chem. Phys.* **1963**, *39*, 1397. Whangbo, M.; Hoffman, R. *J. Am. Chem. Soc.* **1978**, *100*, 6093.

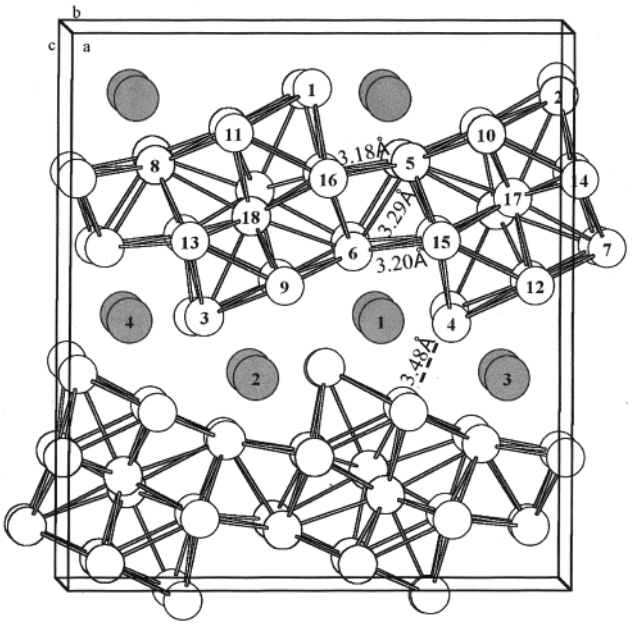

Figure 1. ~[100] section of the unit cell of monoclinic Sc_9Te_2. The pairs of similar but independent metal atoms within the 3 × 3 columns that alternate down the short *a* axis (1−2, 3−4, 5−8, 6−7, 9−12, 10−11, 13−15, 14−16, 17−18), as marked on separate columns. White atoms are scandium; gray atoms are tellurium.

cluster block can be described as the side-by-side condensation product of four infinite trans-edge-sharing chains of octahedra. (Note in the figure that the shared edge (waist) and vertex positions alternate by *a*/2, with the waist of the octahedron assigned to the clearly shorter trans distance.) Similar infinite chains of condensed octahedra have been useful in the earlier description of Sc−Sc bonding in Sc_2Te, Sc_8Te_3, and Sc_7Cl_{10},[23] where possible close-packed or condensed bcc features are less apparent. Each column here is bonded to parallel units on opposed faces (at atoms 5, 6, 15, and 16) by another chain of edge-sharing octahedra to generate corrugated sheets of these columns normal to $\vec{c}$. The latter connections, marked in Figure 1, range over 3.18−3.29 Å, while edges on the opposing column faces (6−16 and 5−15) are much shorter, 3.05 Å. The shortest metal−metal distance between sheets, 3.48 Å (4−11), is marked in Figure 1, although the corresponding overlap population is relatively small (below).

Significant distortions in this structure relative to Ti_9Se_2 occur along the individual columns, and these are better seen in Figure 2 in which the chain axis ($\vec{a}$) is horizontal. This pattern is comprised of four crystallographically distinct octahedra, two "squashed" (18, 9, 13, 12, 15, 3; 17, 16, 11, 14, 10, 2) and two more regular octahedra (18, 11, 16, 14, 10, 1; 17, 12, 15, 9, 13, 4), with the latter highlighted. The distances within one of each type of octahedron are marked in Figure 2, those in the other pair being fairly similar. The Sc−Sc distances around the more regular octahedron vary from 3.1 to 3.3 Å, with waists of ~3.5 Å (9−12 or 13−15) and heights of 4.4 Å (4−17). Distances around the squashed octahedra vary from 3.1 to 3.4 Å, with shorter height distances of ~3.5 Å (marked, 2−17) and longer waists of ~4.3 Å (10−11, 14−16), along the chain, that is, compressed by about 0.8 Å so that the height and waist proportions of the octahedra have been reversed but remain comparable. One regular and one squashed octahedron share a vertex (17,18) and are connected via two shared edges along $\vec{a}$ to another such pair with the distortion reversed with respect to the first one. In this way, the regular octahedra in this view occupy opposed positions across the chain, in concert with the alternation of squashed octahedra. Finally, the sides on these chains of octahedra are augmented by metal atoms (5,8; 6,7) that simultaneously cap faces of adjoining octahedra and squashed octahedra and define bridges to the adjoining column, Figure 1. The distances to the shared vertexes of the octahedra are fairly constant, slightly less than 3.4 Å (5−17, 7−17, 6−18, 8−18). All tellurium atoms are located within tricapped trigonal prismatic scandium figures, with Sc−Te distances in a 2.9−3.2-Å range. Appropriate to the electron richness of this compound, all Te−Te distances are 4.0 Å or greater and nonbonding.

The parent from which this zigzag pattern of distorted octahedra can be derived is shown in Figure 3, the undistorted, or structurally averaged, Sc_9Te_2 that corresponds to the Ti_9Se_2-type structure.[9] Here, the waists and heights of the octahedra are both ~3.9 Å, quite long for good bonding, and the overall column structure is just a simple but rather extensive condensation of these. The observed superstructure is achieved by splitting the five independent metal positions into four or two sites each, as keyed with a superscript for the former sites on the atom numbers in Table 2. The descent in space group symmetry from *Pbam* for Ti_9Se_2 to *Cc* for Sc_9Te_2 is not direct, but is predicted to require two steps,[24] so the transition must be first-order rather than continuous. The major displacements, marked in Figure 3 by arrows, occur along the short $\vec{a}$ axis,

Table 3. Sc−Sc Distances (Å) and Corresponding Overlap Populations (OP)

atom 1	atom 2	distance	OP	i,e[a]	atom 1	atom 2	distance	OP	i,e[a]
7	8	3.00	0.363	i1	14	16	3.45	0.153	i3
14	17	3.00	0.306	i2	13	15	3.47	0.149	i3
13	18	3.00	0.305	i2	10	11	3.49	0.145	i3
15	18	3.01	0.298	i2	9	12	3.49	0.142	i3
16	17	3.01	0.298	i2	6	12	3.23	0.141	e1
6	16	3.05	0.274	i1	6	9	3.24	0.140	e1
5	15	3.05	0.273	i1	5	10	3.25	0.137	e1
6	14	3.05	0.273	i1	5	11	3.25	0.137	e1
9	18	3.11	0.272	i2	4	15	3.18	0.137	e1
5	13	3.06	0.272	i1	5	16	3.18	0.133	e1
12	18	3.12	0.268	i2	5	14	3.19	0.132	e1
10	17	3.12	0.267	i2	4	13	3.20	0.130	e1
11	17	3.13	0.263	i2	6	15	3.20	0.130	e1
16	18	3.13	0.233	i2	6	13	3.19	0.130	e1
15	17	3.14	0.229	i2	1	16	3.21	0.127	e1
14	18	3.15	0.226	i2	1	14	3.24	0.120	e1
13	17	3.15	0.224	i2	3	13	3.29	0.114	e1
5	6	3.29	0.214	i1	4	12	3.30	0.112	e1
12	17	3.22	0.213	i2	4	9	3.32	0.108	e1
9	17	3.23	0.209	i2	1	11	3.31	0.108	e1
11	18	3.24	0.206	i2	3	15	3.32	0.108	e1
8	13	3.26	0.204	i1	2	14	3.32	0.106	e1
11	16	3.25	0.204	i1	3	9	3.36	0.104	e1
7	14	3.26	0.203	i1	1	10	3.33	0.104	e1
8	15	3.27	0.202	i1	2	10	3.35	0.104	e1
10	14	3.25	0.202	i2	9	16	3.60	0.103	i2
10	18	3.25	0.201	i2	12	14	3.60	0.103	i2
7	16	3.27	0.201	i1	7	13	3.34	0.102	e1
12	15	3.26	0.200	i2	8	14	3.34	0.100	e1
9	13	3.26	0.199	i2	2	11	3.37	0.100	e1
7	12	3.11	0.182	e1	3	12	3.38	0.100	e1
7	9	3.11	0.181	e1	2	16	3.34	0.100	e1
7	17	3.36	0.179	i2	7	15	3.34	0.100	e1
8	11	3.13	0.176	e1	11	13	3.62	0.100	i2
6	18	3.37	0.176	i2	10	15	3.62	0.099	i2
10	8	3.13	0.175	e1	8	16	3.35	0.098	e1
5	17	3.39	0.171	i2	17	18	3.93	0.041	i3
8	18	3.38	0.170	i2	4	11	3.48	0.025	e2
3	18	3.43	0.164	i2	4	10	3.49	0.024	e2
2	17	3.46	0.155	i2					

[a] i = interior Sc−Sc bond: i1, inside 3 × 3 column; i2, inside the octahedral chain shared between columns; i3, along short axis repeat. e = exterior: e1, on exterior of 3 × 3 block; e2, interlayer.

(23) Poeppelmeier, K. R.; Corbett, J. D. *Inorg. Chem.* **1977**, *16*, 1107.

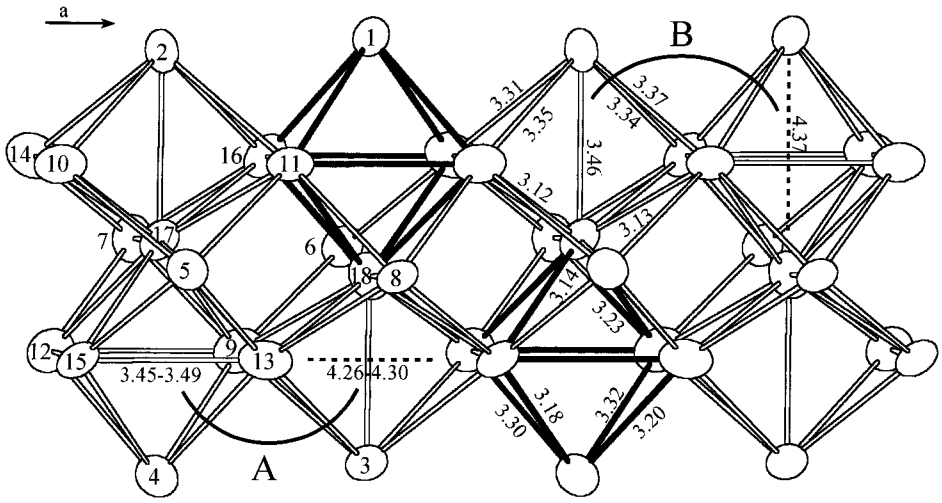

Figure 2. The repeating pattern of shared, distorted, octahedra along the short *a* axis of Sc_9Te_2 drawn with 99% probability thermal ellipsoids and distances marked in Å. The darker bonds emphasize the zigzag arrangement of octahedra, and the arcs, the alternating octahedral waist (A) and height (B) pattern.

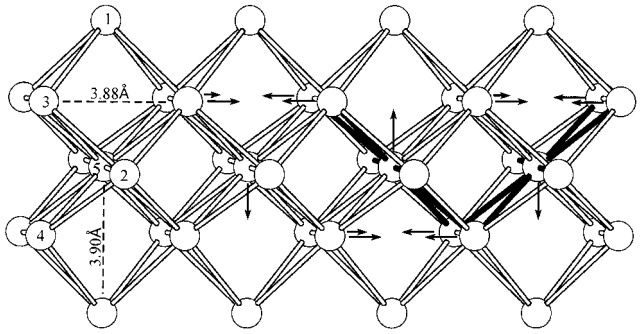

Figure 3. A view along the short *a* axis of the ideal undistorted, or structurally averaged, Sc_9Te_2 in the orthorhombic Ti_9Se_2 structure type. The average distances of the waist and height dimensions of the octahedra are marked as well as the metal displacement pattern that produces the observed distorted structure in Figure 2.

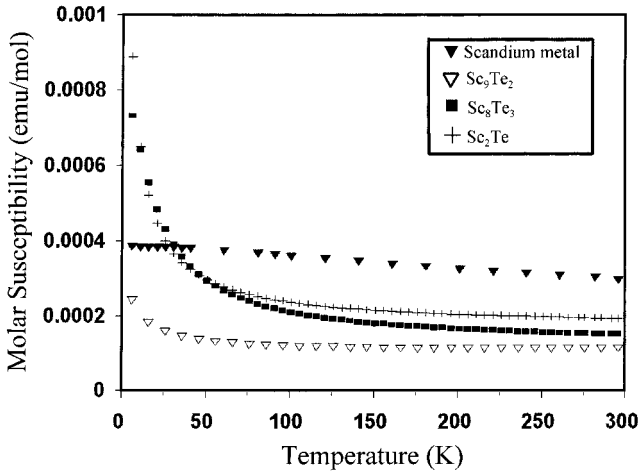

Figure 4. Molar magnetic susceptibilities per scandium versus temperature for Sc_9Te_2, other scandium-rich tellurides, and the metal.

while neighboring columns displace out of phase so as to yield a doubled *b* axis as well (Figure 1).

Physical Properties. Sc_9Te_2 exhibits a paramagnetic susceptibility with a small temperature dependence at the lowest temperatures, as shown in Figure 4 along with data for other metal-rich scandium phases for comparison, all as χ/mol of Sc. The temperature dependence here is much less than those observed for both Sc_2Te and Sc_8Te_3, and the result is quite Pauli-like from 50−300 K. The room-temperature susceptibility of scandium metal[27] is 2−4 times greater than that for any of the scandium-rich tellurides investigated, with Sc_9Te_2 being the lowest. What is different is that the two other scandium-rich phases have greater temperature dependencies at lower temperatures. High-frequency measurements of the resistivity of the polycrystalline Sc_9Te_2 phase over 100−300 K show metallic behavior. The resistivity is ~220 $\mu\Omega$·cm at 298 K, 4 times that of the metal, with a temperature dependence of −0.57% K^{-1}, characteristic of a metallic compound. Neither χ or ρ gave any evidence for a phase transition over the temperature regions studied.

Theoretical Calculations. Although the metal−metal bonded nature of Sc_9Te_2 suggests delocalization of conduction electrons, the unusual distortions away from the more symmetrical Ti_9Se_2 type also suggest electronic driving forces. Band calculations seem necessary to understand this aspect better. Figure 5 shows the total DOS and the total Sc−Sc COOP curve (sum of overlap-weighted bond populations) for Sc_9Te_2 as functions of energy. As is usual for such compounds, the Fermi level is located on the low-energy side of a large conduction band that is composed almost entirely of scandium d and s states. The COOP curve shows that these are highly bonding up to and beyond E_F, which is typical for these electron-deficient compounds. Figure 5 suggests the valence electrons are delocalized within a broad conduction band, but it does not give any hint about the distortion.

We have already seen many examples in which overlap populations may not vary inversely with metal−metal distances, particularly when their locations within a low-dimensional network are distinctly different.[17,18] However, an analysis of all of the individual distances and Sc−Sc overlap populations

(24) Group theoretical methods[25,26] predict that the descent in symmetry involves at least two steps: a transition corresponding to the U_1 irreducible representation of *Pbam* ($k = a^* + c^*/2$) to give $Cmc2_1$ followed by another transition at the Γ_4 point of $Cmc2_1$ ($k = 0$) to yield *Cc*. However, the first step does not meet the Lifshitz criterion and may not be continuous. One could reverse the order of the transitions, which would make $P2_1/c$ the intermediate, and the second step would be unallowed by the Lifshitz criterion.

(25) Stokes, H. T.; Hatch, D. M. *Isotropy Subgroups of the 230 Crystallographic Space Groups*; World Scientific Publishing Co.: Singapore, 1988.

(26) Franzen, H. F. *Physical Chemistry of Solids;* World Scientific Publishing Co.: Singapore, 1994.

(27) Spedding, F. H.; Croat, J. J. *J. Chem. Phys.* **1973**, *59*, 2451.

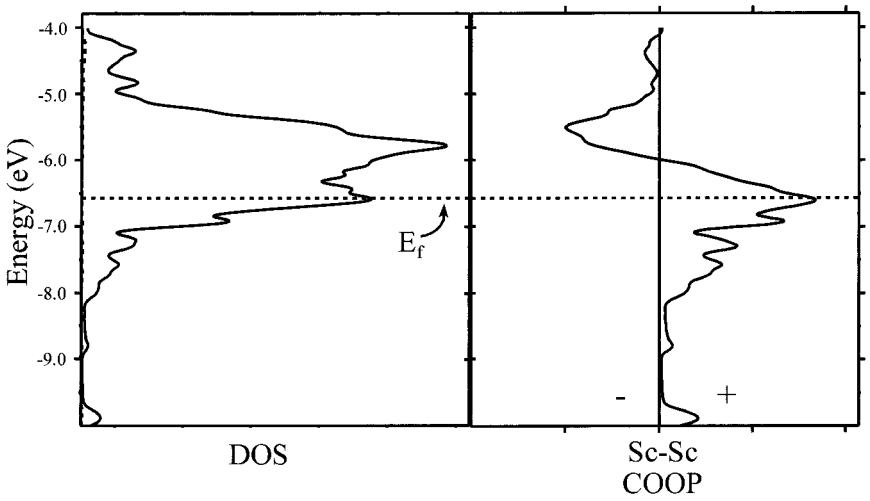

Figure 5. Total densities of states (DOS) (left) and Sc−Sc crystal orbital overlap population (COOP) (right) curves for Sc_9Te_2. The minute Te contributions (dashed) are projected out in the former.

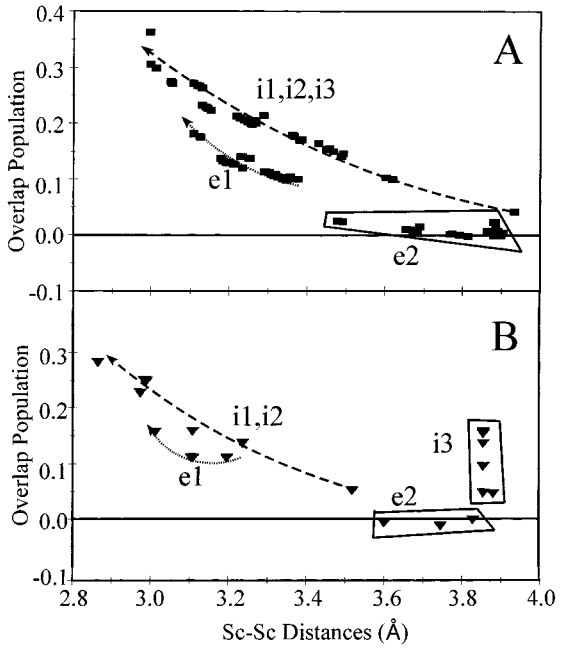

Figure 6. Sc−Sc overlap populations versus distances for the real Sc_9Te_2 structure (A) and for the equivalent undistorted Ti_9Se_2 aristotype (B). Note the clear distinction in A between interior (i) and exterior (e) bond populations within the layer of bridged columns. The categories i3 and e2 refer to values along the short axis and between layers, respectively (see Table 3).

in this complex structure would be cumbersome. Table 3 lists the Sc−Sc distances under 4.0 Å that have overlap populations above 0.02, along with a key to describe the location of each in the structure. The Sc−Sc overlap populations are listed in descending order, and the first 20−30, all of which lie within the chains, parallel increases in distances fairly well. Notable deviations then begin to occur everywhere on the list, depending on the environment of the metal−metal bond. For example, the overlap population for the atom pair 7−12 (0.182) occurs very low on the list considering its distance (3.11 Å), but this bond occurs on the periphery of the 2D sheet. Contrastingly, that for 5−6 (0.214) lies high on the list for its distance (3.29 Å), but this bond occurs between columns within the 2D sheet. This correlation is summarized in Figure 6, part A, where all of the independent Sc−Sc overlap populations are plotted as a function of distance. The data fall basically into two distinct populations, corresponding to either internal or surface (exterior) Sc−Sc bonding. Those for internal Sc−Sc bonds in and between columns, labeled i1 and i2, respectively (following Table 3), together with data for the shortest axial repeats i3 all fall on the upper empirical curve with higher overlap populations for the corresponding distances. The surface and interlayer (exterior) Sc−Sc bonds with Te neighbors (e1 and e2, respectively) occur on a lower curve and have lower overlap populations for their distances. Although we have seen such qualitatively parallel trends before,[17,18] this clear segregation of the Sc−Sc bonds in Sc_9Te_2 into internal and external bond classes has never been quite so conspicuous and compelling. The usual explanation has been that metal-based electrons on Sc atoms with anionic tellurium near neighbors are repelled or, equivalently, that the d states on these metal atoms are raised (the atoms become relatively oxidized) through mixing with Te states. Thus, metal bonds located on the external part of the aggregate follow a different bond order−bond length relationship than those located within the metal aggregates.

Because the Sc_9Te_2 structure is a distorted version of the Ti_9Se_2 structure type, it seemed necessary to determine whether there are conspicuous bonding differences between the two structure types that might justify the distortion. The same calculations were therefore performed for Sc_9Te_2 with an undistorted, or structurally averaged, Ti_9Se_2-type structure. The lower half (B) of Figure 6 shows the same plot of Sc−Sc overlap populations versus distances, with the number of data points greatly reduced because of the higher symmetry of the structure. Again, the Sc−Sc bonding is differentiated into the two categories, interior and exterior distances, but to a lesser extent. A significant difference is that some of the populations for internal Sc−Sc bonding along the short *a* axis (grouped as i3) are relatively large, given their distances, compared with the other internal bondings (i1, i2) and with that in the real structure. This distinction was noted as well in the electron-poorer compounds Sc_2Te and Sc_8Te_3 with ∼1D blades and 2D sheets, respectively. The distortion essentially disproportionates the strong ∼3.9-Å bonds along the short axis, $\vec{a}$, into shorter and stronger ∼3.5-Å bonds well up on the curve in Figure 6A, and longer inconsequential separations near 4.3 Å (off-scale) (Figure 2). Such distortions should be spontaneous given the logarithmic dependence of bond order on distance if the elastic energies and bonding changes elsewhere in the structure are not too important. The distortion in general raises the curve of overlap

populations as a function of distance, curve i1, i2 in Figure 6B lying closer to e1, the exterior populations in the real structure, Figure 6A, than to the curve defined by interior bonding i1, i2, and i3. In other words, the distortion has logically emptied the moderate or less bonding states in the Ti_9Se_2 arrangement while lowering the energy of those that are more bonding. The effects are difficult to discern with only a collective COOP curve comparison. There are appreciable changes during this distortion, however, and over 80 distinct Sc−Sc contacts would need separate analysis. The symmetry reduction found for Sc_9Te_2 relative to a Ti_9Se_2-type aristotype may take place at elevated temperatures, but it must occur above 1135 °C where the crystals were grown.

Such a differentiation does not occur for Sc_8Te_3, which occurs in a Ti_8Se_3 structure type but with clear responses to the larger anion and smaller number of valence electrons. On the other hand, the interior metal positions for Y_8Te_3 refine with somewhat extreme thermal ellipsoids, suggestive of a missing superstructure, but no evidence for this can be found.[28] Some incommensurate behavior may be possible.

Conclusions

The structure of Sc_9Te_2 consists of distorted 3×3 columns of scandium metal that extend infinitely down the *a* axis and are joined laterally into 2D layers along the *b* axis. A corrugated layer of tellurium atoms separates the rumpled metal layers in the $\vec{c}$ direction. The Sc_9Te_2 structure is the result of distortion of the Ti_9Se_2 structure type with doubled *a* and *b* axes and alternating long and short Sc−Sc distances along the columns. Extended Hückel calculations show that the distortion to lowered symmetry generates more regular Sc−Sc bond order−distance relationships (Figure 6A) that clearly distinguish between inner and outer positions on the metal columns or layers.

Acknowledgment. We thank Jerry Ostenson for the magnetic susceptibility measurements and Ilia Guzei for help with the CCD diffractometer. This work was supported by the National Science Foundation, Solid State Chemistry, via Grants DMR-9510278 and DMR-9809850 and was carried out in the facilities of the Ames Laboratory, U.S. Department of Energy.

Supporting Information Available: Tables of additional crystallographic and refinement parameters, anisotropic thermal parameters, and a complete listing of nearest neighbor distances. This material is available free-of-charge via the Internet at http//pubs.acs.org. See any current masthead page for ordering information and Web access instructions.

JA993316J

(28) Maggard, P. A.; Corbett, J. D., unpublished results.